Int. J. Heat Mass Transfer. Vol. 36, No. 9, pp. 2349–2358, 1993
Printed in Great Britain

0017–9310/93 $6.00 + 0.00

A study of the effects of macrosegregation and buoyancy-driven flow in binary mixture solidification

S. K. SINHA,† T. SUNDARARAJAN‡ and V. K. GARG§‖

† Department of Mechanical Engineering, Delhi Institute of Technology, Kashmere Gate, Delhi 110006, India
‡ Department of Mechanical Engineering, Indian Institute of Technology, Kanpur 208016, India
§ NASA Lewis Research Center, Mail Stop 5-11, 21000 Brookpark Road, Cleveland, OH 44135-3191, U.S.A.

(*Received* 27 *January* 1992 *and in final form* 16 *September* 1992)

Abstract—A generalized anisotropic porous medium approach is developed for modelling the flow, heat and mass transport processes during binary mixture solidification. Transient predictions are obtained using FEM, coupled with an implicit time-marching scheme, for solidification inside a two-dimensional rectangular enclosure. A parametric study focusing attention on the effects of solutal buoyancy and thermal buoyancy is presented. It is observed that three parameters, namely the thermal Rayleigh number (Ra_H), the solutal Rayleigh number (Ra_F) and the relative density change parameter (σ_2), significantly alter the flow fields in the liquid and the mushy regions. Depending upon the nature of these flow fields, the solute enrichment caused by macrosegregation may occur on the top or the bottom region of the enclosure.

INTRODUCTION

MACROSEGREGATION is an important phenomenon that is known to occur during the solidification of a mixture. Indeed, it is primarily responsible for the concentration variation of the dissolved component in the solidified material. For metal alloys, the mechanical properties such as strength are profoundly influenced by this phenomenon. In the past, several authors have made attempts to develop simplified models for alloy solidification by neglecting the diffusion and advection of solute and assuming that a homogeneous material undergoes a phase-change within a given range of temperatures [1–5]. In these works, the mushy zone has been modelled as a porous medium and a suitable Darcy source term is added to the momentum equation so as to gradually extinguish the velocities as the liquid solidifies. Though this model can explain several important physical phenomena for dilute alloys, it fails to predict macrosegregation which is commonly observed if the alloy is not very dilute.

The early studies to analyse the process of solute transport [6–9] are based on simplistic models. In these studies, macrosegregation was considered to be unidirectional. Hence, while tendencies for both positive and negative segregation have been predicted, these methods do not have a general applicability. In recent years, many comprehensive models have been developed which are capable of predicting macrosegregation in the most general cases [10–16]. The models are primarily based on the continuum mixture theory or on the local volume-averaging method. The mixture theory views the mushy zone as an overlapping continuum, which is occupied by the solid and the liquid simultaneously. On the other hand, in the volume-averaging approach, the mushy zone is conceived to consist of two interpenetrating phases; the classical conservation equations are applied only within each phase but not over the entire mixture. The details of these approaches can be found in refs. [13, 15, 17].

Although the phenomenon of macrosegregation of a solute has been studied by many authors in recent years, the relative roles played by the thermal buoyancy (due to the temperature gradient) and the solutal buoyancy (due to the concentration gradient) upon macrosegregation have not been highlighted so far. In the present study, the solidification of a binary mixture inside a two-dimensional rectangular geometry has been analysed, with a particular view to identifying the nature of the flow processes and the associated mass transfer due to macrosegregation.

MATHEMATICAL FORMULATION

The solidification process of the binary alloy system can be described in terms of the flow, heat transfer and solutal transport in the solid, mushy and liquid zones. In addition, appropriate models are necessary for representing the property variation in the mush and also for determining the volume fraction of liquid (or porosity) as a function of the concentration and temperature. It is also important to determine the permeability values based upon the morphology of

‖ Author to whom all correspondence should be addressed.

NOMENCLATURE

c specific heat
D^{α} coefficient of diffusion of solute
f^{α}, F mass fraction of solute (dimensional and non-dimensional)
g acceleration due to gravity
h specific enthalpy
h_l^0 latent heat of phase-change at $T = 0$
h_f latent heat of phase-change at T_e
k thermal conductivity
k_p equilibrium partition ratio
K permeability tensor
K_1, K_2 components of K in principal directions
L width of the cavity
Le Lewis number
m, M morphology parameter (dimensional and non-dimensional)
Pr Prandtl number
p, P dynamic pressure (dimensional and non-dimensional)
R non-dimensional porous medium resistivity tensor defined by equation (6)
R_{xx}, R_{xy}, R_{yx}, R_{yy} components of R in the global Cartesian coordinate system
Ra_f solutal Rayleigh number
Ra_θ thermal Rayleigh number
Ste Stefan number
t time
T temperature
T_m fusion temperature for $f^{\alpha} = 0$
u, v, U, V components of superficial velocity (dimensional and non-dimensional)
x, y, X, Y Cartesian coordinates (dimensional and non-dimensional).

Greek symbols
α thermal diffusivity
β_s solutal expansion coefficient
β_T thermal expansion coefficient
γ angle made by the local gradient of temperature with the x-axis
ε porosity (volume fraction of liquid)
θ non-dimensional temperature
μ viscosity
ν kinematic viscosity
ρ density
$\sigma_1, \ldots, \sigma_9$ non-dimensional variables defined by equation (19)
τ non-dimensional time
$\Delta\tau$ non-dimensional time-step.

Subscripts
c cold wall
e eutectic
h hot wall
i initial condition
l liquid or liquidus
0, ref reference values
s solid or solidus.

Superscripts
* non-dimensional normalized value
α solute.

the dendrite structure and finally relate them to the local porosity values. The governing equations have to be solved in a transient manner, starting from known initial conditions.

The generalized governing equations for the solid, mushy and liquid regions pertaining to binary alloy solidification are given by the expressions described below [5, 14]. In these expressions, the porosity and the velocity values are equal to zero in the solid region, while the porosity varies from zero to one in the mushy zone and becomes unity in the liquid region. Also, the permeability at each point in the mushy zone has been treated as a second order tensor due to anisotropy. Other porous medium properties such as equivalent thermal conductivity and solute diffusivity have been taken as isotropic, for the sake of simplicity. The governing equations are:

Continuity

$$\frac{\partial}{\partial t}\left(\frac{\rho}{\rho_l}\right) + \frac{\partial u}{\partial x} + \frac{\partial v}{\partial y} = 0. \quad (1)$$

X-momentum

$$\frac{\rho}{\rho_l}\frac{\partial}{\partial t}\left(\frac{\rho_l}{\rho}u\right) + u\frac{\partial}{\partial x}\left(\frac{\rho_l}{\rho}u\right) + v\frac{\partial}{\partial y}\left(\frac{\rho_l}{\rho}u\right) = -\frac{1}{\rho_l}\frac{\partial p}{\partial x} + \nu_l\left[\frac{\partial}{\partial x}\left\{\frac{\rho}{\rho_l}\frac{\partial}{\partial x}\left(\frac{\rho_l}{\rho}u\right)\right\} + \frac{\partial}{\partial y}\left\{\frac{\rho}{\rho_l}\frac{\partial}{\partial y}\left(\frac{\rho_l}{\rho}u\right)\right\}\right] - \frac{\nu_l}{m}(R_{xx}u + R_{xy}v). \quad (2)$$

Y-momentum

$$\frac{\rho}{\rho_l}\frac{\partial}{\partial t}\left(\frac{\rho_l}{\rho}v\right) + u\frac{\partial}{\partial x}\left(\frac{\rho_l}{\rho}v\right) + v\frac{\partial}{\partial y}\left(\frac{\rho_l}{\rho}v\right) = -\frac{1}{\rho_l}\frac{\partial p}{\partial y} + \nu_l\left[\frac{\partial}{\partial x}\left\{\frac{\rho}{\rho_l}\frac{\partial}{\partial x}\left(\frac{\rho_l}{\rho}v\right)\right\} + \frac{\partial}{\partial y}\left\{\frac{\rho}{\rho_l}\frac{\partial}{\partial y}\left(\frac{\rho_l}{\rho}v\right)\right\}\right] - \frac{\nu_l}{m}(R_{yx}u + R_{yy}v) + g\{\beta_T(T - T_{ref}) + \beta_s(f_l^{\alpha} - f_{ref}^{\alpha})\}. \quad (3)$$

Energy

$$\frac{\partial}{\partial t}(\rho h)+\rho_l\left(u\frac{\partial h_l}{\partial x}+v\frac{\partial h_l}{\partial y}\right)=\frac{\partial}{\partial x}\left(k\frac{\partial T}{\partial x}\right)+\frac{\partial}{\partial y}\left(k\frac{\partial T}{\partial y}\right)+h_l\frac{\partial \rho}{\partial t}. \quad (4)$$

Species

$$\frac{\partial}{\partial t}(\rho f^\alpha)+\rho_l\left(u\frac{\partial f_l^\alpha}{\partial x}+v\frac{\partial f_l^\alpha}{\partial y}\right)=\frac{\partial}{\partial x}\left(\varepsilon\rho_l D_l^\alpha\frac{\partial f_l^\alpha}{\partial x}\right)+\frac{\partial}{\partial y}\left(\varepsilon\rho_l D_l^\alpha\frac{\partial f_l^\alpha}{\partial y}\right)+f_l^\alpha\frac{\partial \rho}{\partial t} \quad (5)$$

where f^α, f_l^α are the solute (α) mass fractions of the mixture and the liquid, respectively. While deriving the species transport equation (5), it has been assumed that the solute diffusivity in solid phase, $D_s^\alpha \simeq 0$. In equations (2) and (3), R_{xx}, R_{xy}, R_{yx} and R_{yy} are the components of a tensor R, which is given by

$$R = mK^{-1} \quad (6)$$

where K is the anisotropic permeability tensor and m a morphology constant. The principal values of the permeability tensor, in turn, can be approximately estimated through the expressions [5, 18]

$$K_1 = \frac{m\varepsilon^3}{(1-\varepsilon)^2} \quad (7a)$$

and

$$K_2 = \frac{m\varepsilon^3}{(1-\varepsilon)^{0.75}}. \quad (7b)$$

Assuming that the primary dendrite growth occurs along the direction of the local temperature gradient in the mushy zone, the following relations can be derived for the components of R:

$$R_{xx} = m\left(\frac{K_1+K_2}{2K_1K_2}-\frac{K_1-K_2}{2K_1K_2}\cos 2\gamma\right) \quad (8a)$$

$$R_{yy} = m\left(\frac{K_1+K_2}{2K_1K_2}+\frac{K_1-K_2}{2K_1K_2}\cos 2\gamma\right) \quad (8b)$$

$$R_{xy} = R_{yx} = -m\frac{K_1-K_2}{2K_1K_2}\sin 2\gamma \quad (8c)$$

where

$$\tan\gamma = \frac{\partial T}{\partial y}\Big/\frac{\partial T}{\partial x}. \quad (8d)$$

One of the key aspects of the equivalent porous medium formulation for the mushy zone is the choice of appropriate representation for the variation of properties. For instance, the viscosity appearing in the momentum equations is usually chosen as the liquid viscosity. The density ρ, thermal conductivity k, specific heat c, enthalpy h and mass fraction of solute f^α are mixture properties which are evaluated through the lever rule applied between the solid and the liquid phases, yielding

$$\rho = \varepsilon\rho_l+(1-\varepsilon)\rho_s \quad (9a)$$

$$k = \varepsilon k_l+(1-\varepsilon)k_s \quad (9b)$$

$$c = \frac{\varepsilon\rho_l c_l+(1-\varepsilon)\rho_s c_s}{\rho} \quad (9c)$$

$$h = \frac{\varepsilon\rho_l h_l+(1-\varepsilon)\rho_s h_s}{\rho} \quad (9d)$$

and

$$f^\alpha = \frac{\varepsilon\rho_l f_l^\alpha+(1-\varepsilon)\rho_s f_s^\alpha}{\rho} \quad (9e)$$

where

$$h_s = c_s T \quad (9f)$$

$$h_l = c_l T+h_l^0 \quad (9g)$$

$$h_l^0 = (c_s-c_l)T_e+h_f. \quad (9h)$$

In the present work, it is assumed that k_l, k_s, c_l, c_s and ρ_s are constants, while ρ_l varies with temperature as well as the solute concentration. Invoking the Boussinesq approximation, this variation of ρ_l is accounted for only in the thermal buoyancy and the solutal buoyancy terms of the y-momentum equation. The application of the lever rule to the mixture concentration in the above form (equation (9e)) implies local equilibrium and infinite rate of diffusion of solute within each phase [14, 16] over microscopic volumes at every location in the mushy zone. It is to be borne in mind, however, that the volume fraction of liquid, ε, in the above expressions is yet to be determined. An important assumption which has been put forward in this regard is that of a fixed partition ratio between the liquid and solid phases for the solute concentration, in the whole range of temperature for which solidification occurs. This can be represented as

$$k_p = \frac{f_s^\alpha}{f_l^\alpha}. \quad (10)$$

Taking the variation of both f_s^α and f_l^α with temperature as linear, it can be shown that the liquid fraction ε is given by

$$\varepsilon = \frac{\rho}{\rho_l}\left\{1-\frac{1}{1-k_p}\left(1-\frac{T_m-T_e}{T_m-T}\frac{f^\alpha}{f_e^\alpha}\right)\right\}. \quad (11)$$

The solute fraction in the liquid and the solid phase can, in turn, be determined from the following expressions:

$$f_l^\alpha = \frac{T_m-T}{T_m-T_e}f_e^\alpha \quad (12a)$$

$$f_s^\alpha = \frac{T_m-T}{T_m-T_e}f_e^\alpha k_p. \quad (12b)$$

It is evident from the above expressions that the solute concentrations in the liquid and solid phases cannot

be treated as independent variables in the mushy zone. Thus, the solute transport equation in the mushy zone can be rewritten in terms of temperature as

$$\frac{\partial}{\partial t}(\rho f^{\alpha}) = \frac{\rho_l f_e^{\alpha}}{T_m - T_e}\left(u\frac{\partial T}{\partial x} + v\frac{\partial T}{\partial y}\right) + \frac{\partial}{\partial x}\left(\frac{\varepsilon\rho_l D_l^{\alpha} f_e^{\alpha}}{T_e - T_m}\frac{\partial T}{\partial x}\right) + \frac{\partial}{\partial y}\left(\frac{\varepsilon\rho_l D_l^{\alpha} f_e^{\alpha}}{T_e - T_m}\frac{\partial T}{\partial y}\right) + \frac{T_m - T}{T_m - T_e} f_e^{\alpha}\frac{\partial \rho}{\partial t} \quad (13)$$

while, for pure phases, equation (5) can be used to predict the rate of solute transport. Also, in the y-momentum equation for the mushy zone, f_l^{α} in the solute-buoyancy term can be expressed in terms of temperature. With these assumptions, the non-dimensional equations are given by:

Continuity

$$\frac{\partial \sigma_1}{\partial \tau} + \frac{\partial U}{\partial X} + \frac{\partial V}{\partial Y} = 0. \quad (14)$$

X-momentum

$$\sigma_1\frac{\partial}{\partial \tau}\left(\frac{U}{\sigma_1}\right) + U\frac{\partial}{\partial X}\left(\frac{U}{\sigma_1}\right) + V\frac{\partial}{\partial Y}\left(\frac{U}{\sigma_1}\right) = -\frac{\partial P}{\partial X} + Pr\left[\frac{\partial}{\partial X}\left\{\sigma_1\frac{\partial}{\partial X}\left(\frac{U}{\sigma_1}\right)\right\} + \frac{\partial}{\partial Y}\left\{\sigma_1\frac{\partial}{\partial Y}\left(\frac{U}{\sigma_1}\right)\right\}\right] - M(R_{XX}U + R_{XY}V). \quad (15)$$

Y-momentum

pure phases:

$$\sigma_1\frac{\partial}{\partial \tau}\left(\frac{V}{\sigma_1}\right) + U\frac{\partial}{\partial X}\left(\frac{V}{\sigma_1}\right) + V\frac{\partial}{\partial Y}\left(\frac{V}{\sigma_1}\right) = -\frac{\partial P}{\partial Y} + Pr\left[\frac{\partial}{\partial X}\left\{\sigma_1\frac{\partial}{\partial X}\left(\frac{V}{\sigma_1}\right)\right\} + \frac{\partial}{\partial Y}\left\{\sigma_1\frac{\partial}{\partial Y}\left(\frac{V}{\sigma_1}\right)\right\}\right] - M(R_{YX}U + R_{YY}V) + Ra_{\theta}\,Pr\,\theta + Ra_F\,Pr\,F \quad (16a)$$

mush:

$$\sigma_1\frac{\partial}{\partial \tau}\left(\frac{V}{\sigma_1}\right) + U\frac{\partial}{\partial X}\left(\frac{V}{\sigma_1}\right) + V\frac{\partial}{\partial Y}\left(\frac{V}{\sigma_1}\right) = -\frac{\partial P}{\partial Y} + Pr\left[\frac{\partial}{\partial X}\left\{\sigma_1\frac{\partial}{\partial X}\left(\frac{V}{\sigma_1}\right)\right\} + \frac{\partial}{\partial Y}\left\{\sigma_1\frac{\partial}{\partial Y}\left(\frac{V}{\sigma_1}\right)\right\}\right] - M(R_{YX}U + R_{YY}V) + (1-\sigma_2)Ra_{\theta}\,Pr\,\theta + \sigma_3. \quad (16b)$$

Energy

pure phases:

$$\sigma_4\frac{\partial \theta}{\partial \tau} + U\frac{\partial \theta}{\partial X} + V\frac{\partial \theta}{\partial Y} = \frac{\partial}{\partial X}\left(k^*\frac{\partial \theta}{\partial X}\right) + \frac{\partial}{\partial Y}\left(k^*\frac{\partial \theta}{\partial Y}\right) \quad (17a)$$

mush:

$$\sigma_4\frac{\partial \theta}{\partial \tau} + U\frac{\partial \theta}{\partial X} + V\frac{\partial \theta}{\partial Y} = \frac{\partial}{\partial X}\left(k^*\frac{\partial \theta}{\partial X}\right) + \frac{\partial}{\partial Y}\left(k^*\frac{\partial \theta}{\partial Y}\right) + \sigma_6\frac{\partial \sigma_1}{\partial \tau} - \sigma_5\frac{\partial \varepsilon}{\partial \tau}. \quad (17b)$$

Species

pure phases:

$$\sigma_1\frac{\partial F}{\partial \tau} + U\frac{\partial F}{\partial X} + V\frac{\partial F}{\partial Y} = \frac{\partial}{\partial X}\left(\sigma_7\frac{\partial F}{\partial X}\right) + \frac{\partial}{\partial Y}\left(\sigma_7\frac{\partial F}{\partial Y}\right) \quad (18a)$$

mush:

$$\sigma_1\frac{\partial F}{\partial \tau} = -\sigma_8\left(U\frac{\partial \theta}{\partial X} + V\frac{\partial \theta}{\partial Y}\right) + \frac{\partial}{\partial X}\left(\sigma_7\sigma_8\frac{\partial \theta}{\partial X}\right) + \frac{\partial}{\partial Y}\left(\sigma_7\sigma_8\frac{\partial \theta}{\partial Y}\right) + \sigma_9\frac{\partial \sigma_1}{\partial \tau} \quad (18b)$$

where

$$X = \frac{x}{L},\quad Y = \frac{y}{L},\quad U = \frac{uL}{\alpha_0},\quad V = \frac{vL}{\alpha_0},\quad \tau = \frac{\alpha_0 t}{L^2},$$

$$P = \frac{pL^2}{\rho_l \alpha_0^2},\quad \theta = \frac{T - T_{ref}}{T_h - T_c},\quad F = \frac{f^{\alpha} - f_{ref}^{\alpha}}{f_e^{\alpha} - f_l^{\alpha}},\quad M = \frac{\nu_l L^2}{m\alpha_0},$$

$$Pr = \frac{\nu_l}{\alpha_0},\quad \alpha_0 = \frac{k_0}{\rho_l c_l},\quad k^* = \frac{k}{k_0},\quad \nu_l = \frac{\mu_l}{\rho_l},$$

$$Ra_{\theta} = \frac{gL^3\beta_T(T_h - T_c)}{\alpha_0\nu_l},\quad Ra_F = \frac{gL^3\beta_s(f_e^{\alpha} - f_l^{\alpha})}{\alpha_0\nu_l},$$

$$\sigma_1 = \frac{\rho}{\rho_l},\quad \sigma_2 = \frac{\beta_s f_e^{\alpha}}{\beta_T(T_m - T_e)},$$

$$\sigma_3 = \frac{gL^3\beta_s}{\alpha_0^2}\left(\frac{T_m - T_{ref}}{T_m - T_e}f_e^{\alpha} - f_{ref}^{\alpha}\right),\quad \sigma_4 = \frac{\rho c}{\rho_l c_l},$$

$$\sigma_5 = \frac{(\rho_l c_l - \rho_s c_s)T + \rho_l h_l^0}{\rho_l c_l(T_h - T_c)},\quad \sigma_6 = \frac{c_l T + h_l^0}{c_l(T_h - T_c)},$$

$$\sigma_7 = \frac{\varepsilon}{Le},\quad Le = \frac{\alpha_0}{D_l^{\alpha}},\quad \sigma_8 = \frac{(T_h - T_c)f_e^{\alpha}}{(T_e - T_m)(f_e^{\alpha} - f_l^{\alpha})},$$

$$\sigma_9 = \frac{(T_m - T)f_e^{\alpha} - (T_m - T_e)f^{\alpha}}{(T_m - T_e)(f_e^{\alpha} - f_l^{\alpha})}. \quad (19)$$

During computations, it was assumed that $\rho_l = \rho_s$, $c_l = c_s$ and $k_l = k_s$. Thus, $\sigma_1 = \sigma_4 = k^* = 1.0$ and $\sigma_5 = h_f/c_l(T_h - T_c) = Ste$ (Stefan number). Of the many non-dimensional parameters which arise in the problem, the parameters whose variation forms the focus of the present investigation are Ra_{θ}, Ra_F and σ_2.

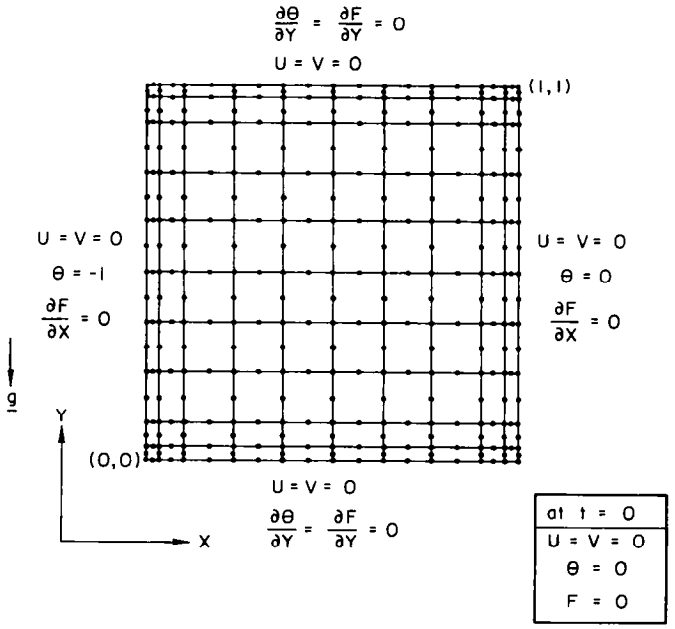

FIG. 1. Problem geometry and numerical grid.

While Ra_θ and Ra_F represent the contributions of the thermal buoyancy and the solutal buoyancy, respectively, σ_2 signifies the relative change in density due to concentration and temperature variations in the mushy zone. The values of other parameters used during the computations are: $k_p = 0.25$, $Le = 10$, $M = 10^6$, $Pr = 0.1$, $Ste = 0.5$, $\sigma_3 = 0$, $\sigma_8 = -1$, $\theta_m = 0.5$, $\theta_c = -1.5$, $F_c = 1.0$, $\theta_c = -1$ and $\theta_h = 0$.

The boundary and initial conditions prescribed for the problem are shown in Fig. 1. The governing equations have been solved numerically by the finite element method coupled with an implicit time-marching procedure. A 10×10 non-uniform grid with eight-noded rectangular elements has been used, as shown in Fig. 1. Galerkin's weighted residual approach has been employed for deriving the matrix equations from the differential equations. The details of the numerical scheme and the tests for the grid-sensitivity of the results are discussed elsewhere [4]. The CPU time taken for a typical run was of the order of 3 min per time-step on a network of HP-9000 series computers. Typically, a non-dimensional time-step value of $\Delta\tau = 0.001$ was used in computations.

COMPARISON WITH EXISTING RESULTS

In spite of the wide attention that the solidification problems have received to date, there are no ready data available on the solidification rates of alloy materials which are suitable for comparison with numerical predictions. For this reason, it has not been possible to validate the numerical predictions against experimental data or analytical solutions pertaining to alloy solidification. However, a check on the accuracy of the predictions can be made by recovering, as a limiting case, results corresponding to pure material solidification, for which extensive data exists in literature.

A comparison of present predictions with the experimental and theoretical results of Beckermann and Viskanta [19] is shown in Fig. 2, for the melting of gallium. In order to simulate the pure metal phase-change, the difference between the dimensionless liquidus and solidus temperatures was prescribed to be very small ($\theta_l - \theta_s = 0.01$) for obtaining the results of the present analysis. It is observed that the shapes of the liquid–solid interface at steady-state predicted by our analysis agree well with those obtained by Beckermann and Viskanta [19] for different con-

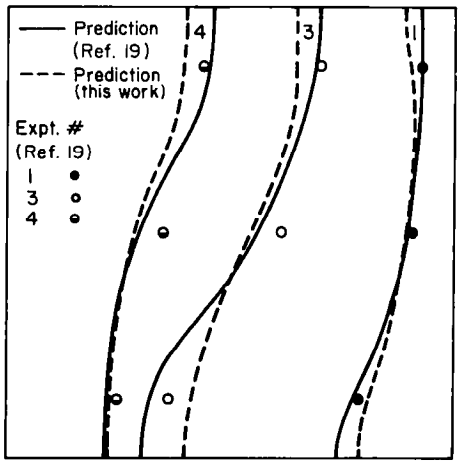

FIG. 2. Comparison of mean interface positions at steady-state with earlier results.

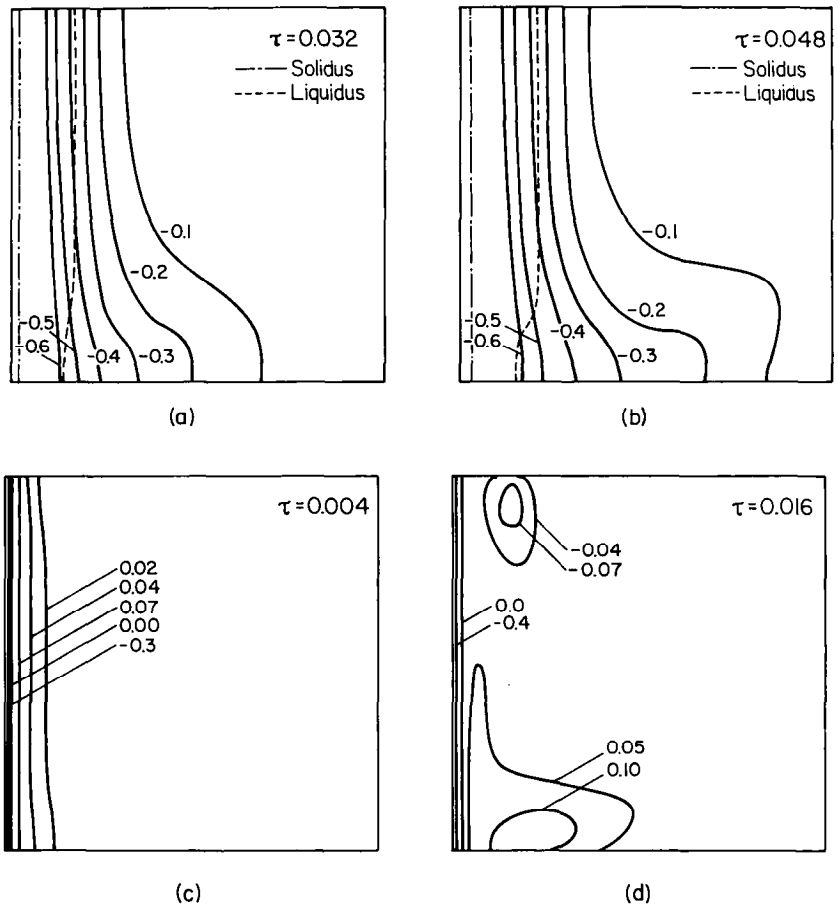

FIG. 3. Progress of solidification for $Ra_\theta = Ra_F = 10^5$, $\sigma_2 = 2$. (a) and (b) isotherms; (c) and (d) isoconcentration lines.

ditions. The small deviations existing between the results may be attributed to the fact that the densities and specific heats of the two phases have been taken to be equal in the present work, while Beckermann and Viskanta have considered slightly different property values for each phase.

DISCUSSION

In the present study, the transient variation of temperature, concentration and velocity fields have been obtained for various ranges of parameters. The important effects which have been highlighted are the influ-

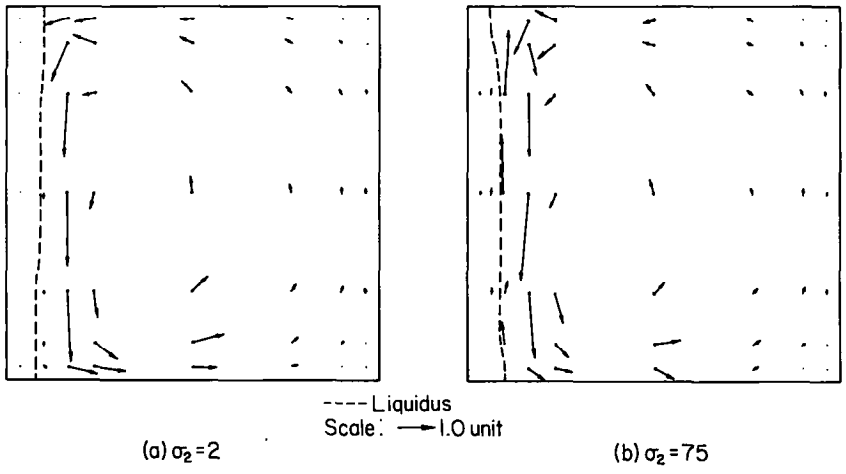

FIG. 4. Influence of solute density variation upon velocity fields: lighter solute ($\sigma_2 > 0$); $Ra_\theta = Ra_F = 10^5$, $\tau = 0.016$.

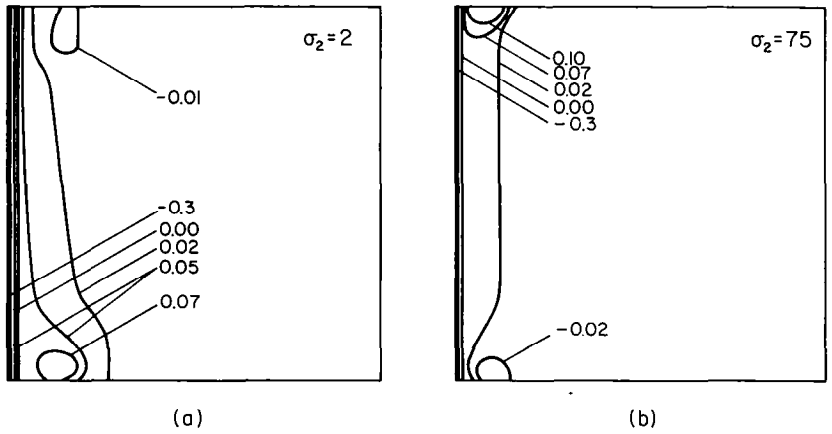

FIG. 5. Influence of solute density variation upon concentration profiles: lighter solute ($\sigma_2 > 0$): $Ra_0 = Ra_F = 10^5$, $\tau = 0.008$.

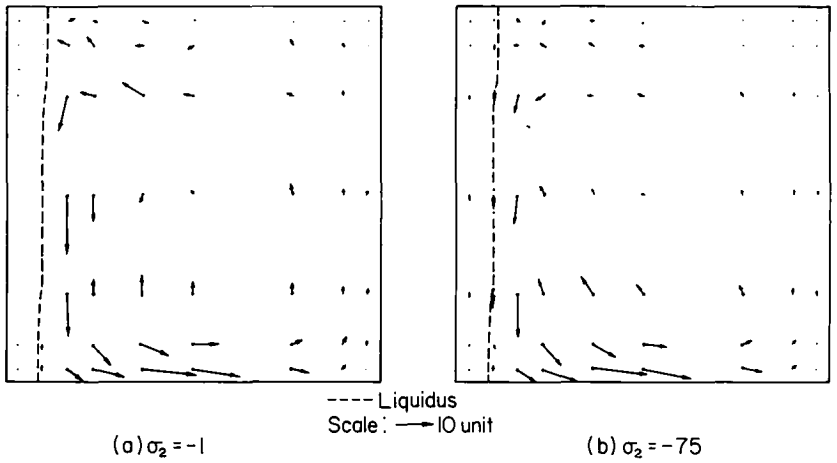

FIG. 6. Influence of solute density variation upon velocity fields: heavier solute ($\sigma_2 < 0$); $Ra_0 = 10^4$, $Ra_F = (-)10^6$, $\tau = 0.016$.

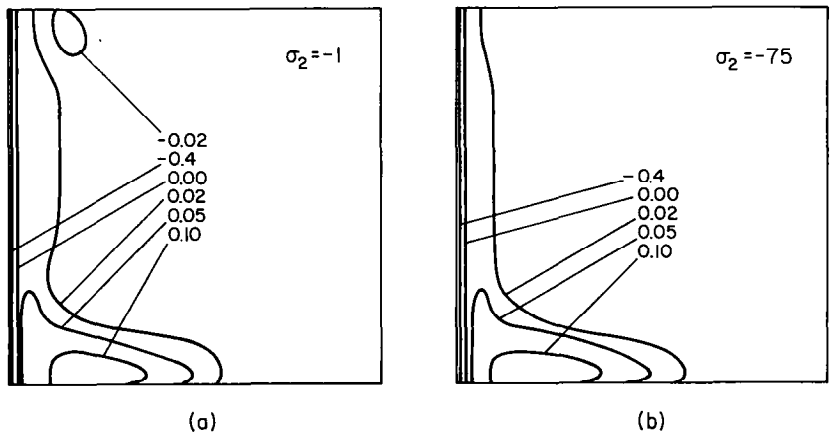

FIG. 7. Influence of solute density variation upon concentration profiles: heavier solute ($\sigma_2 < 0$); $Ra_0 = 10^4$, $Ra_F = (-)10^6$, $\tau = 0.016$.

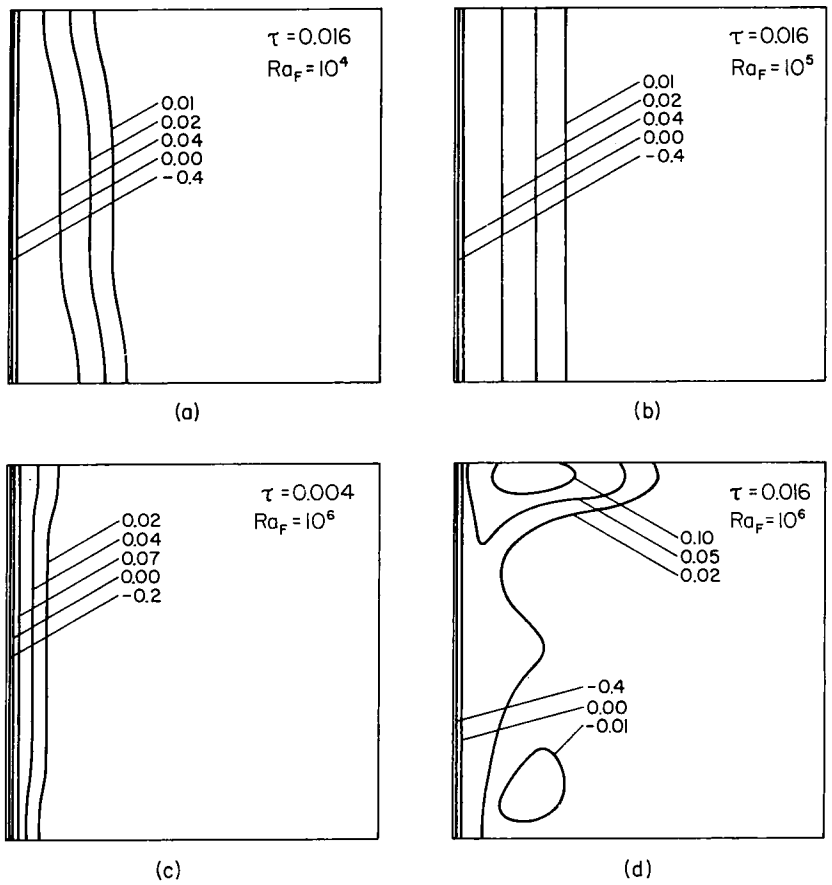

FIG. 8. Effect of solutal Rayleigh number upon concentration profiles; $Ra_0 = 10^4$, $\sigma_2 = 2$.

ence of solutal/thermal Rayleigh numbers upon the flow field and macrosegregation, and also the role played by the ratio of density variation due to temperature and concentration differentials.

Progress of solidification

In Figs. 3(a) and (b), the isotherms have been plotted at two time levels. The relative positions of the liquidus ($\varepsilon = 1$) and the solidus ($\varepsilon = 0$) are shown for the sake of reference. It is seen that the isotherms are curved more in the bottom region towards the hot wall. This clearly indicates the effect of the convective circulation which has anti-clockwise sense for the set of parameters used in the figure. Although both the thermal and solutal Rayleigh numbers are equal, the dimensionless concentration is uniform initially and varies mildly across the liquid region as time proceeds, due to macrosegregation. Indeed, such a mild variation leads to only a minor influence of solutal buoyancy upon the flow field. Thus, the convective circulation as well as the shapes of the isotherms are governed only by thermal buoyancy effects. More discussion on the flow field patterns is presented later. Another interesting feature which is observed from the figures is that the mushy region increases in size with time, due to the increasing difference between the liquidus and solidus temperatures. This trend is also a consequence of the liquid becoming richer in solute as compared to the solid.

The iso-concentration lines for the solute are plotted in Figs. 3(c) and (d) at two different times. Since the dimensionless initial concentration is taken to be zero, negative values of concentration imply depletion, while positive values correspond to enrichment. For small times, the iso-concentration lines are not very curved even in the liquid region, although the enrichment and depletion of the solute across the mushy zone is apparent. For later times, the iso-concentration lines in the liquid region become highly distorted. It is interesting to note that enrichment occurs at the bottom while depletion in liquid occurs at the top. Although a positive value of σ_2 implies that the solute is lighter than the liquid, the strong thermally driven flow confines the enriched fluid to the bottom region near the solidification front. The depleted zone in liquid at the top of the cavity is believed to be a consequence of remelting of solid when it comes in contact with circulating hot fluid.

Influence of solute density variation

The parameter σ_2 gives the ratio of liquid density variation due to change in solutal concentration and

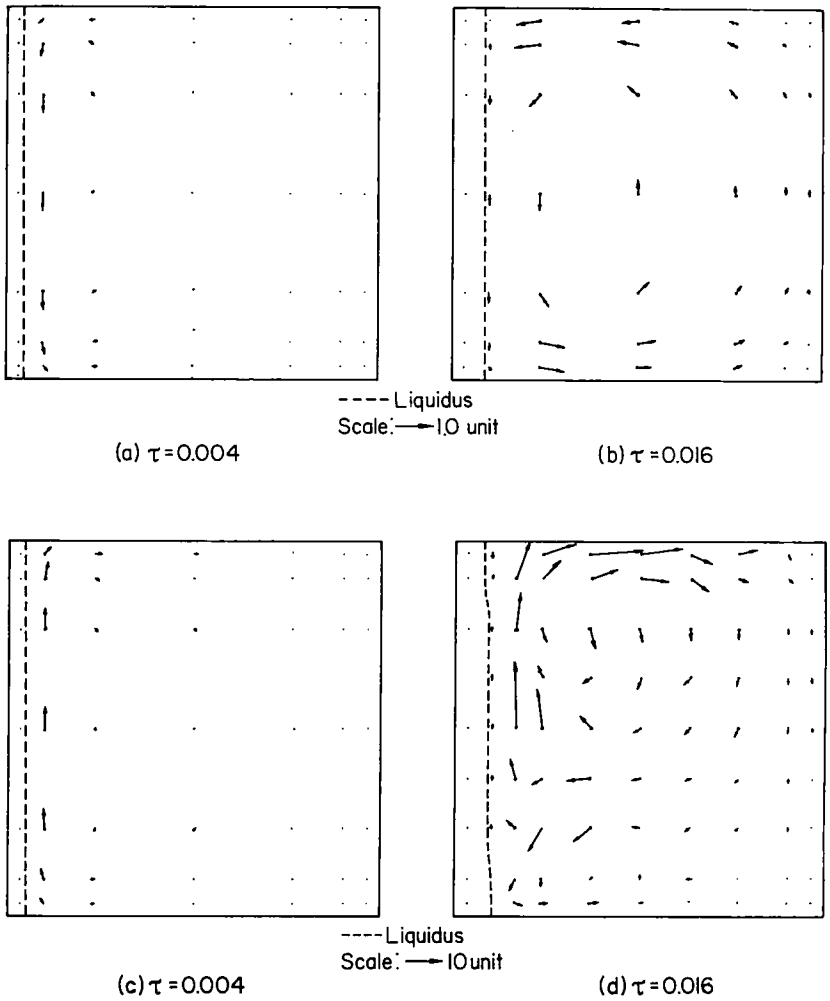

FIG. 9. Velocity fields for (a) and (b) predominant thermal buoyancy, $Ra_\theta = 10^4$, $Ra_F = 10^4$, $\sigma_2 = 2$; and (c) and (d) predominant solutal buoyancy, $Ra_\theta = 10^4$, $Ra_F = 10^6$, $\sigma_2 = 2$.

that due to temperature change. A large positive value of σ_2 would occur if the solute is very much lighter than the solvent. On the other hand, a large negative value of σ_2 pertains to the situation when the solute is much heavier. The effects of σ_2 upon the flow field and the concentration profiles are discussed below.

In Figs. 4(a) and (b), the velocity fields are shown for $\sigma_2 = 2$ and 75. Although the flow field in the liquid region is largely unaffected by σ_2, the flow within and adjacent to the mushy zone is significantly altered, with the emergence of a circulation pattern which is counter to the thermally driven field for a large positive value of σ_2. The shape of the liquidus is also modified when the parameter σ_2 is increased. These features can be explained from the facts that the solute is lighter compared to the solvent in the present case and a strong solutal buoyancy which opposes the thermally driven flow occurs for $\sigma_2 = 75$ in the vicinity of the mushy region due to macrosegregation. In Figs. 5(a) and (b), the concentration profiles for the two values of σ_2 are plotted for the same time level. While enrichment at the bottom and depletion at the top occurs for $\sigma_2 = 2$, the trend is exactly reversed for $\sigma_2 = 75$. These trends are obviously determined by the fact that the thermally driven flow is predominant in the former situation, while solutal buoyancy effects gain strength near the mushy zone in the latter case.

For negative values of σ_2, the thermal and the solutal buoyancy effects are in the same direction in and around the mushy zone (see Figs. 6 and 7). The only difference between small or large negative values of σ_2 is that the flow velocities are large in magnitude inside the mushy zone also, for the latter case as compared to the former. An additional feature which is observed for $\sigma_2 = -1$ is the presence of a small clockwise vortex at the top portion. This can be attributed to the depletion of solute which is observed in Fig. 7(a). Except for this small depleted region, the isoconcentration lines are more or less similar in both the cases. The presence of such solute depleted/enriched liquid zones has been observed by other investigators as well [14, 16] at high Rayleigh numbers.

Effect of solutal Rayleigh number

The iso-concentration lines for different solutal Rayleigh numbers are shown in Figs. 8(a)–(d). It is observed that the advancement of the iso-concentration lines is faster in the bottom region at $Ra_F = 10^4$ while it is equal at bottom and top for $Ra_F = 10^5$, and slower at the bottom region for $Ra_F = 10^6$. In all these cases, the thermal Rayleigh number has been maintained constant at 10^4. These features reflect the nature of the flow field, which changes from anti-clockwise sense of circulation to a clockwise circulation, as Ra_F is increased from 10^4 to 10^6. For $Ra_F = 10^6$ and large times, enrichment and depletion of solute occurs at the top and bottom regions, respectively, as is dictated by the sense of circulation.

The flow fields for two different values of Ra_F are shown in Figs. 9(a)–(d). It is evident from these figures that the sense of circulation changes when Ra_F is increased from 10^4 to 10^6. An interesting point to note is that for small times, the initiation of circulation occurs close to the solidifying region in all the cases presented. While the trend for larger Ra_F values can be easily explained in terms of macrosegregation across the mushy region, the observation requires some detailed explanation for $Ra_F = 10^4$. In the present study, the initial temperature of fluid is taken to be the same as that of the hot wall and, at time $\tau = 0^+$, the temperature of $\theta = -1$ is imposed at $x = 0$. The cooling of fluid which results from this sudden imposition of boundary condition at $x = 0$ results in a downward flow being generated adjacent to the solidifying region. Elsewhere within the cavity, the velocity values are negligibly small for small times. An examination of the magnitude of velocity vectors indicates that flow is vigorous in the anti-clockwise sense for $Ra_F = 10^4$, and in the clockwise sense for $Ra_F = 10^6$. In the former case, it is thermally driven flow, while in the latter, it is driven by solutal buoyancy. In all the above figures, the flow is very weak within the mushy zone due to the small value of σ_2 considered herein. For $Ra_F = 10^6$, a minor vortex with a sense of circulation opposite to that of the main vortex is observed in the bottom region. Obviously, this is a consequence of solute depletion in this region.

CONCLUSIONS

A parametric study highlighting the relative roles of solutal buoyancy and thermal buoyancy during binary mixture solidification has been presented. The flow field characteristics in the liquid as well as the mushy regions and their effects upon macrosegregation are discussed in detail. It is observed that the relative density change parameter σ_2 affects the flow pattern in the vicinity of the mushy region. For large positive values of σ_2, a flow whose sense of circulation is opposite to that of the main liquid vortex occurs within the mushy zone, while for negative values of σ_2, the liquid region and mushy zone have the same sense of circulation. For positive σ_2 and a large solutal Rayleigh number, even the main liquid vortex has an opposite sense of rotation as compared to the thermally-driven case. These changes in flow pattern profoundly influence the region of solute enrichment by macrosegregation.

REFERENCES

1. V. R. Voller and C. Prakash, A fixed grid numerical modelling methodology for convection–diffusion mushy region phase change problems, *Int. J. Heat Mass Transfer* **30,** 1709–1719 (1987).
2. S. Chellaiah and R. Viskanta, Freezing of water-saturated porous media in the presence of natural convection : experiments and analysis, *ASME J. Heat Transfer* **111,** 425–432 (1989).
3. W. Shyy and M. H. Chen, Steady-state natural convection with phase-change, *Int. J. Heat Mass Transfer* **33,** 2545–2563 (1990).
4. S. K. Sinha and T. Sundararajan, Analysis of alloy solidification inside arbitrary-shaped two-dimensional enclosures, *Int. J. Heat Mass Transfer* (in press).
5. S. K. Sinha, T. Sundararajan and V. K. Garg, A variable property analysis of alloy solidification using the anisotropic porous medium approach, *Int. J. Heat Mass Transfer* **35,** 2865–2878 (1992).
6. M. C. Flemings and G. E. Nereo, Macrosegregation : Part I, *Trans. TMS-AIME* **239,** 1449–1461 (1967).
7. R. Mehrabian, M. Keane and M. C. Flemings, Interdendritic fluid flow and macrosegregation ; influence of gravity, *Metall. Trans.* **1B,** 3228–3241 (1970).
8. S. Kou, D. R. Poirier and M. C. Flemings, Macrosegregation in electroslag remelted ingots, *Proc. Electr. Furn. Conf., Iron Steel Soc. AIME* **35,** 221–228 (1977).
9. S. D. Ridder, S. Kou and R. Mehrabian, Effect of fluid flow on macrosegregation in axi-symmetric ingots, *Metall. Trans.* **12B,** 435–447 (1981).
10. R. N. Hills, D. E. Loper and P. H. Roberts, A thermodynamically consistent model of a mushy zone, *Q. J. Mech. Appl. Math.* **36,** 505 (1983).
11. V. C. Prantil and P. R. Dawson, Application of a mixture theory to continuous casting. In *Transport Phenomena in Materials Processing* (Edited by M. M. Chen, J. Majumdar and C. L. Tucker), pp. 47–54. ASME, New York (1983).
12. C. Beckermann, Melting and solidification of binary mixtures with double-diffusive convection in the melt, Ph.D. Thesis, Purdue University, West Lafayette (1987).
13. W. D. Bennon and F. P. Incropera, A continuum model for momentum, heat and species transport in binary solid–liquid phase change systems—I. Model formulation, *Int. J. Heat Mass Transfer* **30,** 2161–2170 (1987).
14. V. R. Voller, A. D. Brent and C. Prakash, The modelling of heat, mass and solute transport in solidification systems, *Int. J. Heat Mass Transfer* **32,** 1719–1731 (1989).
15. S. Ganesan and D. R. Poirier, Conservation of mass and momentum for the flow of interdendritic liquid during solidification, *Metall. Trans.* **21B,** 173–181 (1990).
16. G. Amberg, Computation of macrosegregation in an iron–carbon cast, *Int. J. Heat Mass Transfer* **34,** 217–227 (1991).
17. R. Viskanta and C. Beckermann, Mathematical modelling of solidification. In *Multidisciplinary Issues in Materials Processing and Manufacturing* (Edited by S. K. Samanta *et al.*), pp. 501–526. ASME, New York (1987).
18. D. R. Poirier, Permeability for flow of interdendritic liquid in columnar-dendritic alloys, *Metall. Trans.* **18B,** 245–255 (1987).
19. C. Beckermann and R. Viskanta, Effect of solid subcooling on natural convection melting of a pure metal, *ASME J. Heat Transfer* **111,** 416–424 (1989).